APPLIED PHYSICS

Salt-induced ductilization and strain-insensitive resistance of an intrinsically conducting polymer

Hao He[1], Rui Chen[1,2], Shizhong Yue[1], Suzhu Yu[3,4], Jun Wei[4], Jianyong Ouyang[1,5]*

High mechanical ductility and high mechanical strength are important for materials including polymers. Current methods to increase the ductility of polymers such as plasticization always cause a remarkable drop in the ultimate tensile strength. There is no report on the ductilization of polymers that can notably increase the elongation at break while not lowering the ultimate tensile strength. Here, we report the salt-induced ductilization of an intrinsically conducting polymer, poly(3,4-ethylenedioxythiophene):polystyrenesulfonate (PEDOT:PSS). Treating highly conductive PEDOT:PSS with a salt such as sodium perchlorate can enhance its elongation at break from 8.5 to 53.2%, whereas it hardly affects the tensile strength. Moreover, the resistance of the ductilized PEDOT:PSS films is insensitive to the tensile strain before fracture and slightly increases by only ~6% during the cyclic tensile testing with the strain up to 30%. These effects are ascribed to the decrease in the Coulomb attraction between $PEDOT^+$ and PSS^- by the salt ions.

INTRODUCTION

Both high mechanical ductility and high mechanical strength are required for materials in many applications. A brittle material can be easily broken down under mechanical strain, while a soft material without enough strength is often developed with other materials with high mechanical strength to form composites for practical applications. For example, stretchable conductive wires are needed for electronic textiles. As stretchable conductors usually have low mechanical strength, they must be coated on or imbedded into the nonconductive textile. However, the composites can have a high resistivity. A conductive material with high mechanical ductility and high mechanical strength can be directly used as electronic textile without the nonconductive textile.

It is of significance to develop materials with high mechanical ductility and high mechanical strength. However, there is generally a trade-off relationship between the ductility and strength for materials including polymers, metals, and ceramics. It is always a big challenge to achieve both high mechanical ductility and high mechanical strength for the same material. For example, polymers in the glassy state can have high tensile strength but very limited ductility, while in the rubbery state, they can have high ductility but low tensile strength. Plasticization can greatly increase the ductility of polymers but also remarkably lowers the tensile strength. The ideal way is the ductilization of polymers that can saliently increase the elongation at break while hardly affecting the ultimate tensile strength. However, the ductilization has been reported mainly for metals (*1*–*4*). The ductilization is related to the interfacial energy between particles or grains and the matrix. To our best knowledge, there is no report on the ductilization of polymers in literature. The popular ways to increase the elongation at break of polymers including the polymer blend formation (*5*, *6*), plasticization (*7*), and chemical modification (*8*) always noticeably lower the tensile strength. On the other hand, forming a composite with inorganic fillers can usually increase the tensile strength and tensile modulus of a polymer, but it hardly affects or even lowers the elongation at break (*9*, *10*).

Intrinsically conducting polymers (ICPs) have conjugated backbones, and they can have high conductivity in either the oxidized or reduced state. ICPs can have important applications in many areas because they can have the properties of both polymers and metals. For example, ICPs can have important application in electronic textiles and bioelectronics owing to their high mechanical flexibility and biocompatibility (*11*–*15*). However, ICPs are in the glassy state and mechanically brittle at room temperature due to the rigid conjugated backbone and strong interaction between the cations and anions. Their elongation at break is usually less than 10% at room temperature. Several strategies were developed to enhance the elongation at break including blending with a soft or elastomeric polymer (*16*–*18*) and plasticization (*19*, *20*). Nevertheless, these methods can cause a severe drop in the tensile strength. It is essential to endow ICPs with both high tensile strength and high elongation at break because these properties are needed in many applications, such as electronic textiles and electromagnetic shielding (*8*, *16*). Thus, it is significant to develop ICPs with high mechanical ductility and high tensile strength. It is possible to observe high tensile strength and high mechanical ductility on an ICP consisted of a conjugated polyion and a saturated counter polyion like poly(3,4-ethylenedioxythiophene): polystyrenesulfonate (PEDOT:PSS; chemical structure shown in Fig. 1A) because the conjugated polyion can be strong, while the saturated counter polyion can be ductile. However, the strong Columbic attraction between the conjugated polyion and the saturated counter polyion lead to very low ductility. We hypothesize that the Coulombic attraction can be weakened by small cations and anions of a salt, which can associate with the polyanions and polycations of the ICPs, respectively (*21*). As a result, this can greatly increase the elongation of the break of the ICPs. To associate with the polyanions and polycations of the ICPs, the small cations and anions of the salt should not be strongly bound together in the ICPs.

Here, we report the salt-induced ductilization of PEDOT:PSS. A free-standing PEDOT:PSS film treated with ethylene glycol (EG) can exhibit a tensile strength of 23.2 MPa with the elongation at break

[1]Department of Materials Science and Engineering, National University of Singapore, Singapore 117579, Singapore. [2]MOE Key Laboratory of Low-Grade Energy Utilization Technologies and Systems, School of Energy and Power Engineering, Chongqing University, Chongqing 400044, P. R. China. [3]Singapore Institute of Manufacturing Technology, Singapore 637662, Singapore. [4]Harbin Institute of Technology, University Town of Shenzhen, Shenzhen 518055, P. R. China. [5]NUS Research Institute, No 16 South Huashan Road, Liangjiang New Area, Chongqing, China.
*Corresponding author. Email: mseoj@nus.edu.sg

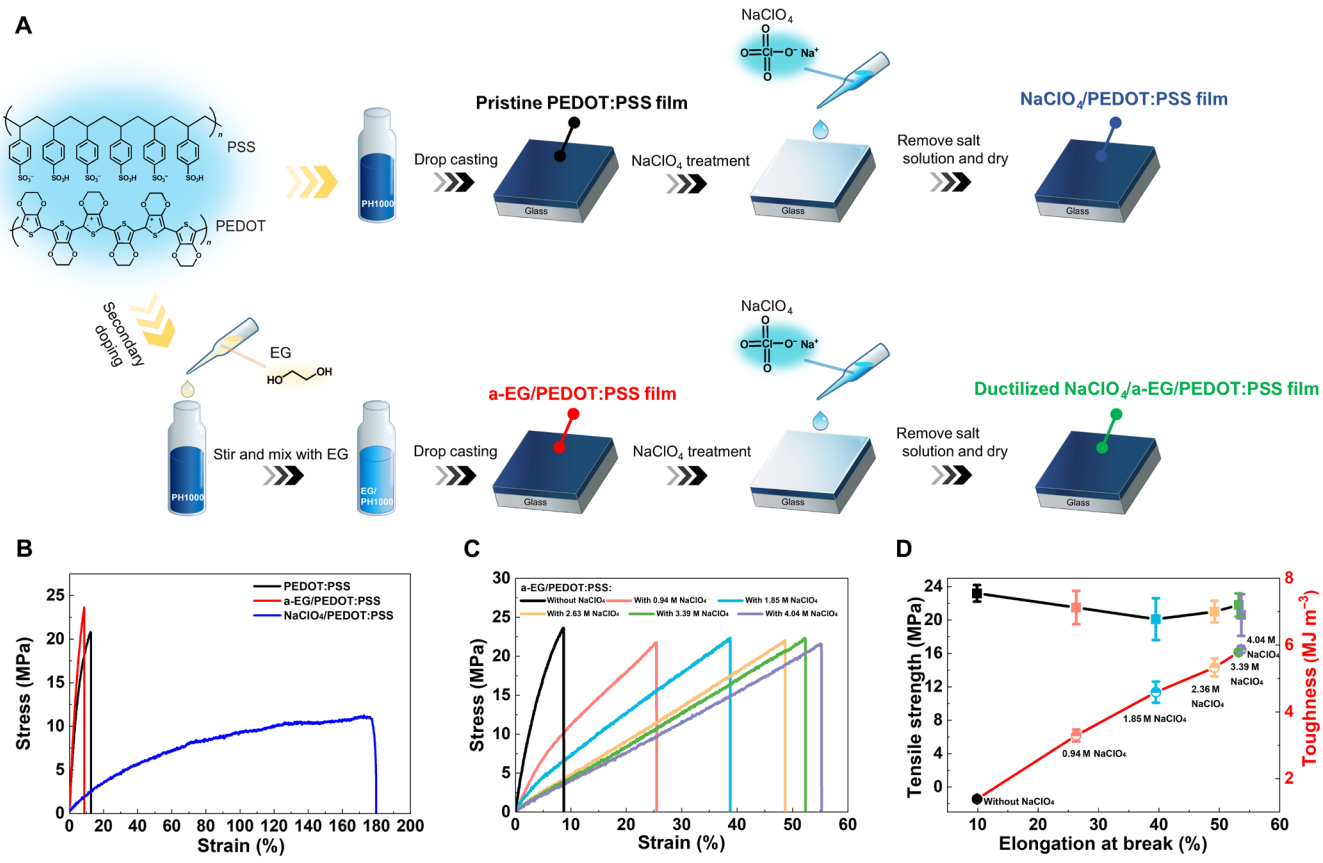

Fig. 1. Fabrication and mechanical properties of PEDOT:PSS with different treatments. (**A**) A schematic illustration for the preparation of PEDOT:PSS, a-EG/PEDOT:PSS, $NaClO_4$/PEDOT:PSS, and a-EG/$NaClO_4$/PEDOT:PSS films. They were peeled from the substrate for the tensile test. (**B**) Stress-strain curves of PEDOT:PSS, a-EG/PEDOT:PSS, and (3.39 M $NaClO_4$)/PEDOT:PSS films. (**C**) Stress-strain curves of an a-EG/PEDOT:PSS film and $NaClO_4$/a-EG/PEDOT:PSS films. The concentrations of the $NaClO_4$ solutions for the treatment are indicated. (**D**) Variations of the toughness and tensile strength of a-EG/PEDOT:PSS and $NaClO_4$/a-EG/PEDOT:PSS films with the elongation at break. The error bars represent the SD, and the tensile rate was 7.1% min^{-1} for the tensile tests.

below 10%. It can be ductilized through a subsequent posttreatment with various salts, including $NaClO_4$, NaCl, NH_4Cl, and $CuCl_2$. The ductilization is related to the lattice energy of the salts and the hydration energy of the salt ions. Among the salts, $NaClO_4$ can give rise to the highest ductilization effect. The salt treatment by $NaClO_4$ can greatly enhance the elongation at break of a-EG/PEDOT:PSS to 53.2% and hardly affects the tensile strength. In addition, the ductilized PEDOT:PSS films can have a conductivity of 538 S cm^{-1}, and they exhibit a resistance insensitive to the tensile strain before fracture. In addition, the resistance slightly increases by only ~6% during the cyclic tensile testing with the tensile strain up to 30%.

RESULTS

Mechanical properties of PEDOT:PSS films

As shown in Fig. 1A, pristine PEDOT:PSS films of ~10 μm in thickness were prepared from its aqueous dispersion (Clevios PH1000) by drop casting. In terms of the tensile measurement, they exhibit an elongation at break of ~10%, a tensile strength of 20.8 MPa, and a Young's modulus of 337 MPa (Fig. 1B). The stress-strain behavior is very different from that of neat poly(4-styrenesulfonic acid) (PSSH) films. As shown in fig. S1, a neat PSSH film exhibits an elongation at break of 42.4%, an ultimate tensile strength of 15.6 MPa at the strain of 29%, and a Young's modulus of 72 MPa. The mechanical brittleness of PEDOT:PSS can be attributed to the stronger Coulomb attraction between $PEDOT^+$ and PSS^-, which leads to the cross-linking of the polymer chains. The higher tensile strength and Young's modulus of PEDOT:PSS than PSSH suggest that the rigid PEDOT chains form continuous networks via π-π stacking in PEDOT:PSS (*22*). There are PEDOT-rich and PSS-rich domains in pristine PEDOT:PSS. The simulation by Zozoulenko and colleagues (*23*) indicates that the PEDOT-rich domains are connected by the PEDOT chains. This is also consistent with the conductivity of pristine PEDOT:PSS that is about 0.4 S cm^{-1} because the conductivity arises from the PEDOT networks.

The pristine PEDOT:PSS films were then treated with $NaClO_4$ by dropping an aqueous solution of $NaClO_4$ on the films (Fig. 1A). After 12 hours at room temperature, the PEDOT:PSS films were spun to remove the solution, and they were then dried at ambient conditions for 6 hours. Free-standing $NaClO_4$/PEDOT:PSS films were obtained by peeling off from the substrate. The thicknesses of the PEDOT:PSS films before and after the treatment with $NaClO_4$ are listed in table S1. The specimens for the tensile test have a width of 1.5 mm and a length of 7 mm unless specified. This $NaClO_4$ treatment can markedly improve the elongation at break to 180%. However, it also lowers the tensile strength to 10.9 MPa and the Young's

modulus to 24 MPa (Fig. 1B). These changes are similar to the effects of ionic liquids on the mechanical properties of PEDOT:PSS films (*20*). The Young's modulus of polymers depends on the interchain interaction. The marked decrease in the Young's modulus by $NaClO_4$ suggests the decrease in the interchain interaction of PEDOT:PSS.

Although the $NaClO_4$ treatment greatly affects the mechanical properties, its effect on the conductivity of pristine PEDOT:PSS is small. It lowers the conductivity to ~0.2 S cm^{-1}. This suggests that the $NaClO_4$ treatment may not affect the PEDOT networks too much.

Apart from the mechanical properties, a high conductivity is also required for PEDOT:PSS. It is well known that secondary doping can enhance the conductivity of PEDOT:PSS by several orders in magnitude (*24*). In this work, secondary doping was carried out by adding EG into the aqueous dispersion of PEDOT:PSS (Fig. 1A). The a-EG/PEDOT:PSS (the symbol of "a-EG" is used to represent the addition of EG into the PEDOT:PSS aqueous dispersion) films were prepared by drop-casting and then drying at 120°C for 15 min and successively at 160°C for 15 min. They can exhibit a conductivity of 775 S cm^{-1}. It is higher than that of the pristine PEDOT:PSS prepared from the aqueous solution without EG by three orders in magnitude. As shown in Fig. 1B, this secondary doping with EG only slightly affects the mechanical properties of the PEDOT:PSS films. The elongation at break slightly decreases to 8.5%, and the tensile strength and the Young's modulus slightly increase to 23.2 and 368 MPa, respectively. The effect of EG on the electrical and mechanical properties can be attributed to the enhanced crystallinity of PEDOT arising from the phase segregation of PSSH from PEDOT:PSS because EG can screen the interaction between $PEDOT^+$ and PSS^- during the film formation (*25*, *26*).

The a-EG/PEDOT:PSS films were further posttreated with $NaClO_4$ solutions at room temperature for 12 hours and then dried at room temperature for 6 hours. The $NaClO_4$/a-EG/PEDOT:PSS film is homogeneous and flexible and can be easily manipulated by hand (fig. S2 and movie S1). Figure 1C shows the stress-strain curves of the $NaClO_4$/a-EG/PEDOT:PSS films with the $NaClO_4$ concentration of 4.04 M or lower. The $NaClO_4$ posttreatment can greatly increase the elongation at break. A higher $NaClO_4$ concentration can give rise to higher elongation at break and a more linear relationship between the stress and strain. Although the elongation at break is greatly improved, all $NaClO_4$/a-EG/PEDOT:PSS films exhibit a high tensile strength of ~21 MPa irrespective to the $NaClO_4$ concentration, similar to that of a-EG/PEDOT:PSS.

The stress-strain curve of a soft polymer is usually sensitive to the strain rate. The elongation at break of the $NaClO_4$/a-EG/PEDOT:PSS films only decreases from 52 to 43% when the strain rate is increased from 7.1 to 71% min^{-1}. Although the strain rate can affect the stress-strain curve of $NaClO_4$/a-EG/PEDOT:PSS films, the tensile strength merely increases from 22.3 to 24.6 MPa (fig. S3). This suggests that the mechanical behavior is different from the plastic deformation of general polymers, which is sensitive to the strain rate. The strain rate of 7.1% min^{-1} was adopted for the tensile tests unless specified in this work. The mechanical properties of $NaClO_4$/a-EG/PEDOT:PSS are independent of the film thickness (fig. S4, A and B), and they are almost same for the samples with different dimensions (fig. S4C). The Young's modulus of the $NaClO_4$/a-EG/PEDOT:PSS films decreases with the increasing $NaClO_4$ concentration (fig. S5). The result also suggests that the presence of $NaClO_4$ can affect the interchain interaction of PEDOT:PSS because the Young's modulus is related to the conformational change of the polymer chains under stress, which depends on the interchain interaction.

These results indicate that the $NaClO_4$ treatment is notably different from plasticization. Plasticization can increase the elongation at break while lowering the tensile strength, and the stress-strain curve of a plasticized polymer at high strain is usually very sensitive to the strain rate (*19*, *20*). The effect of $NaClO_4$ on the mechanical properties of a-EG/PEDOT:PSS films indicates the ductilization of the polymer. It can greatly increase the toughness of the PEDOT:PSS films that is the area below the stress-strain curve (Fig. 1D). The toughness of (3.39 M $NaClO_4$)/a-EG/PEDOT:PSS films is more than four times as that of a-EG/PEDOT:PSS films.

Aqueous solutions with higher $NaClO_4$ concentrations were used to treat a-EG/PEDOT:PSS. The saturation concentration of $NaClO_4$ in water is 8.88 M. As shown in fig. S6, when the $NaClO_4$ concentration was increased to 6.59 or 8.88 M, both the elongation at break and the tensile strength of the polymer films become lower than that treated with 4.04 M $NaClO_4$ solution. These changes can be understood by considering the large amount of $NaClO_4$ in the polymer films.

Note that the ductilization of a-EG/PEDOT:PSS is induced by $NaClO_4$ instead of the water of the solution as evidenced by the control experiments of treating a-EG/PEDOT:PSS films with pure water (fig. S7A). A treatment with water only slightly affects the tensile strength and elongation at break. In addition, if a ductile $NaClO_4$/a-EG/PEDOT:PSS film is rinsed with water to remove $NaClO_4$, then its elongation at break drops to less than 10% (fig. S7B).

Although water does not directly ductilize PEDOT:PSS, annealing the $NaClO_4$/a-EG/PEDOT:PSS films can affect the $NaClO_4$ dispersion in PEDOT:PSS and the ductilization. After an as-prepared $NaClO_4$/a-EG/PEDOT:PSS film was annealed at 80°C for 1.5 hours, $NaClO_4$ crystallites can be observed on the sample surface (fig. S8A). It is consistent with the exothermic process revealed by the differential scanning calorimetry of $NaClO_4$/a-EG/PEDOT:PSS (fig. S9). The $NaClO_4$ crystallites disappeared when the annealed sample was stored under ambient conditions with the relative humidity (RH) of 85% for 0.5 hours. Presumably, the annealing effect can be attributed to the dehydration of the Na^+ and ClO_4^- ions in PEDOT:PSS. These ions can be hydrated in as-prepared $NaClO_4$/a-EG/PEDOT:PSS because the ductilization is done with the aqueous solution of $NaClO_4$, and the samples are handled under ambient conditions. Dehydration of the ions can occur during the annealing process, and rehydration can take place under ambient conditions.

The dehydration remarkably affects the mechanical properties of $NaClO_4$/a-EG/PEDOT:PSS. As shown in fig. S8B, the elongation at break and the tensile strength of the annealed $NaClO_4$/a-EG/PEDOT:PSS film decrease to 20.5% and 13 MPa, respectively. After it is subsequently stored under ambient conditions for 0.5 hours, the elongation at break and tensile strength increase to 40.1% and 16 MPa, respectively. Probably, there are still small $NaClO_4$ crystallites in the samples after the storage under ambient conditions, and they induce flaws to the samples. As a result, both the elongation at break and tensile strength are lower than that of the as-prepared sample. The reason may be similar for the lower elongation at break and lower tensile strength of as-prepared $NaClO_4$/a-EG/PEDOT:PSS ductilized with an aqueous solution of 6.59 or 8.88 M $NaClO_4$; the large amount of $NaClO_4$ can lead to the formation of small $NaClO_4$ crystallites and, thus, flaws in the samples.

Samples of a-$NaClO_4$/a-EG/PEDOT:PSS (a-NaClO4 is used to represent the addition of NaClO4 into the a-EG/PEDOT:PSS) were also prepared from the PEDOT:PSS aqueous solution added with EG and $NaClO_4$. They cannot be dried at room temperature because EG has a high boiling point. Instead, the a-$NaClO_4$/a-EG/PEDOT:PSS samples were prepared by drying the solution at 80°C. $NaClO_4$ crystallites can be observed on the dried a-$NaClO_4$/a-EG/PEDOT:PSS sample prepared from the solution of 1.4 weight % (wt %) $NaClO_4$ (fig. S8C), and the sample exhibits an elongation at break of only 17.0% and a tensile strength of 16 MPa (fig. S8D). The a-$NaClO_4$/a-EG/PEDOT:PSS sample prepared from the solution of 0.7 wt % $NaClO_4$ exhibits a higher tensile strength than that of 1.4 wt % $NaClO_4$. This also evidences that the $NaClO_4$ crystallites can induce flaws and thus lower the tensile strength.

The surface scanning electron microscopy (SEM) and energy-dispersive x-ray spectroscopy (EDX) images of Cl, S, and Na indicate that $NaClO_4$ can be uniformly dispersed in the $NaClO_4$/a-EG/PEDOT:PSS films (Fig. 2 and fig. S10). The atomic ratios of Cl/S were determined in terms of the EDX results (fig. S11). The Cl/S ratio increases with the $NaClO_4$ concentration of the solution for the ductilization. In addition, this ratio is almost the same for the surface and cross-sectional area, which implies no excess of $NaClO_4$ on the surface. The Cl/S ratio determined in terms of the EDX result of (3.39 M $NaClO_4$)/a-EG/PEDOT:PSS is consistent with that by the x-ray photoelectron spectroscopy (fig. S12).

The surface morphology of the a-EG/PEDOT:PSS films was studied by the atomic force microscopy (AFM) before and after the ductilization with $NaClO_4$. The AFM phase images indicate that the $NaClO_4$ treatment can lower the phase of a-EG/PEDOT:PSS (Fig. 2, G and H). A high AFM phase indicates a high repulsive force and thus high stiffness (*27*, *28*). The AFM phases of $NaClO_4$/a-EG/PEDOT:PSS and a-EG/PEDOT:PSS films are consistent with their Young's moduli. When neat water is used for the treatment, the AFM phase of the a-EG/PEDOT:PSS film hardly changes (fig. S13). This also evidences that $NaClO_4$ instead of water induces the ductilization of a-EG/PEDOT:PSS.

The x-ray diffraction (XRD) patterns indicate that the $NaClO_4$ treatment can affect the crystallinity of PEDOT:PSS (Fig. 2I). The XRD pattern at ~26° originates from the π-π stacking of the PEDOT chains (*29*). Treating a pristine PEDOT:PSS film with $NaClO_4$ increases the full width at half maximum from 3.3° to 4.3° and decrease the ratio of the peak intensity to the width, which suggests that the PEDOT:PSS films become more amorphous. That is consistent with the increase in the elongation at break by the $NaClO_4$ treatment. The treatment of a pristine PEDOT:PSS film with EG increases the ratio of the peak intensity to the width, and the further treatment with $NaClO_4$ does not affect it. The effect of the EG treatment on the crystallinity can be ascribed to the phase segregation of some soft PSSH chains from PEDOT:PSS (*25*, *26*). a-EG/PEDOT:PSS and $NaClO_4$/a-EG/PEDOT:PSS show higher crystallinity than pristine PEDOT:PSS and $NaClO_4$/PEDOT:PSS, which is in consistence with their mechanical properties (*30*, *31*).

The secondary doping of PEDOT:PSS can be carried out through the posttreatment of PEDOT:PSS films as well (*32*, *33*). The lowercase letter "p" is added as a prefix to indicate the posttreatment. As shown in Fig. 3A, the PEDOT:PSS films by a posttreatment with a chemical agent such as EG, methanesulfuric acid (MSA), or formic acid (FA) exhibit mechanical properties similar to those of a-EG/PEDOT:PSS. The elongation at break is less than 10%, and the tensile

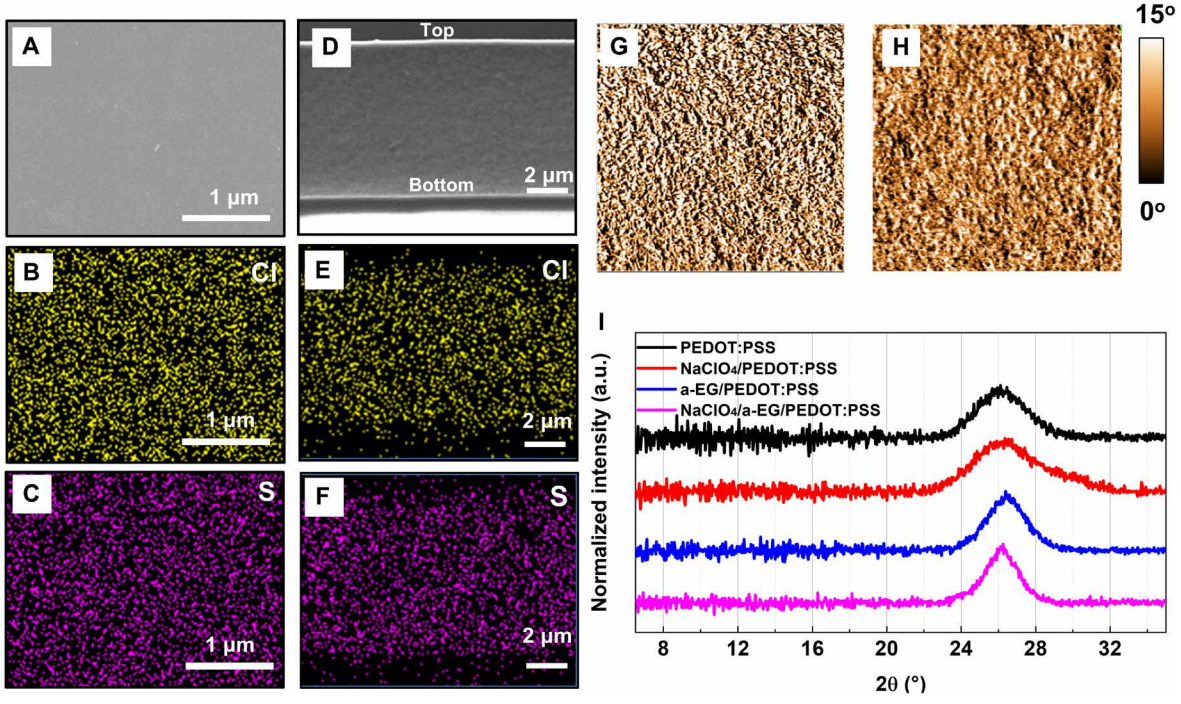

Fig. 2. Characterizations of PEDOT:PSS films. (**A**) Surface and (**D**) cross-sectional SEM images of $NaClO_4$/a-EG/PEDOT:PSS films. (**B** and **C**) Surface and (**E** and **F**) cross-sectional EDX Cl and S mappings of $NaClO_4$/a-EG/PEDOT:PSS films. Atomic force microscopy (AFM) phase images of (**G**) a-EG/PEDOT:PSS and (**H**) $NaClO_4$/a-EG/PEDOT:PSS films. The dimension is 2 μm by 2 μm. (**I**) XRD patterns of PEDOT:PSS films by various treatments. The $NaClO_4$ concentration of the solution for the treatment was 3.39 M. a.u., arbitrary units.

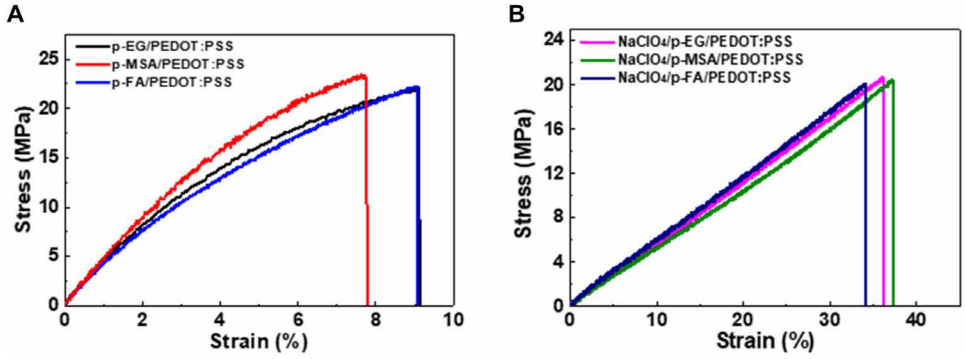

Fig. 3. Mechanical properties of PEDOT:PSS films. Stress-strain curves of (**A**) PEDOT:PSS films posttreated with EG or acids and (**B**) ductilized PEDOT:PSS films. The $NaClO_4$ concentration of the solution was 3.39 M.

strength is 22 to 24 MPa. After they were further treated with $NaClO_4$, the elongation at break increases to 34 to 37%, and the tensile strength hardly changes. These results indicate that $NaClO_4$ can also ductilize these PEDOT:PSS films, which are posttreated with EG, MSA, or FA for the secondary doping (Fig. 3B).

Figure S14 presents the AFM phase images of PEDOT:PSS by various treatments. The AFM phase image of pristine PEDOT:PSS indicates the PEDOT-rich grains with high phase surrounded by PSS-rich domains with low phase (fig. S14A). It is very different from the AFM phase image of PSSH (fig. S14B). The PEDOT:PSS films posttreated with EG or FA before water rinsing exhibit similar AFM images to that of neat PSSH (fig. S14, C and F). This can be attributed to the segregated PSSH on the surface of these films (*34*). The AFM images become very different after the removal of the segregated PSSH chains by water rinsing (fig. S14, D and G). On the other hand, when a PEDOT:PSS film is posttreated with MSA, the segregated PSSH chains are removed from PEDOT:PSS after the treatment because MSA is in the liquid state during the treatment and can dissolve PSSH. As a result, the AFM phase image of p-MSA/PEDOT:PSS is similar to that of p-EG/PEDOT:PSS and p-FA/PEDOT:PSS after water rising (fig. S14I). The two types of grains with different phases become more conspicuous after secondary doping. The grains of high phase is rich of PEDOT, while the ones of low phase is rich of PSS. These results are consistent with that in literature (*29*, *33*, *35*). After the ductilization by $NaClO_4$, the phase of the PEDOT-rich grains decreases, and the boundary between the two types of grains becomes blur (fig. S14, E, H, and J). The change in the AFM phase is consistent with the decrease in the Young's modulus of these polymer films induced by the $NaClO_4$ ductilization.

A treatment of PEDOT:PSS can change its composition and microstructure and can thus affect the electrical and mechanical properties. The PEDOT-to-PSS ratio was studied by the ultraviolet (UV) absorption spectroscopy. As shown in fig. S15, the two absorption peaks at 190 and 225 nm arise from the benzene rings of PSS (*32*). Their intensity drops after the posttreatment with EG, FA, or MSA and further decreases after the $NaClO_4$ ductilization. The absorption intensity at 190 nm was used to estimate the PEDOT-to-PSS mass ratio in the final samples by considering the PEDOT-to-PSS mass ratio of pristine PEDOT:PSS as 0.4 in terms of the composition of the pristine PEDOT:PSS aqueous solution (Table 1). The results indicate that the elongation at break of the ductilized PEDOT:PSS films is related to the PEDOT-to-PSS mass ratio. The $NaClO_4$/a-EG/PEDOT:PSS film has the lowest PEDOT-to-PSS mass ratio of 0.54 but has the highest elongation at break of 53.2%. This ratio increases to 0.72 for the $NaClO_4$/p-EG/PEDOT:PSS and $NaClO_4$/p-FA/PEDOT:PSS films, while their elongation at break decreases to ~35%.

Apart from $NaClO_4$, other salts can also ductilize a-EG/PEDOT:PSS films (Table 1 and fig. S16). The elongation at break of the a-EG/PEDOT:PSS films increases to 30 to 50% after the ductilization with NaCl, NH_4Cl, or $CuCl_2$. These values are lower than that with $NaClO_4$. This indicates that the ions of the salts play important roles in the ductilization of PEDOT:PSS.

In addition, the samples ductilized with different salts show different dependences of their mechanical properties on the humidity of the surrounding. The stress-strain curves of $NaClO_4$/a-EG/PEDOT:PSS are almost the same at the RH of 85 or 25% (figs. S17A). There is no phase separation of $NaClO_4$ at both RHs (fig. S17C). However, the RH can noticeably affect the mechanical properties of NaCl/a-EG/PEDOT:PSS (fig. S17B). The elongation at break of the NaCl/a-EG/PEDOT:PSS film decreases to ~20% at the RH of 25%, which is less than half of that at the RH of 85%. The XRD peaks of NaCl crystals can be obviously observed for the NaCl/a-EG/PEDOT:PSS film stored at the RH of 25% (fig. S17D), and the NaCl crystallites can be observed on the surface by SEM or optical microscope (figs. S18 and S19). Similar phase separation was also observed for NH_4Cl/a-EG/PEDOT:PSS films stored at a low RH.

The $NaClO_4$ ductilization can affect the elasticity of the PEDOT:PSS films as well. In the cyclic tensile testing, the stress at the same strain during the reloading becomes smaller than that during the original loading path (fig. S20), indicating the stress-softening behavior. The ductilized PEDOT:PSS films show high elasticity at small strain. The recovery ratio of $NaClO_4$/a-EG/PEDOT:PSS films is 78.7% at the maximum strain of 10% (Fig. 4A). The recovery of $NaClO_4$/a-EG/PEDOT:PSS is higher than that of free-standing PEDOT:PSS films plasticized with lithium bis(trifluoromethanesulfonyl)imide (LiFTSI) (*20*) or 1-ethyl-3-methylimidazolium 4,5-dicyanoimidazolate (EMIM:DCI) or D-sorbitol (*36*, *37*). It is also higher than the blends of PEDOT:PSS with a soft polymer such as polyvinyl alcohol (PVA) (*18*, *38*) or waterborne polyurethane (WPU) (*11*) (Fig. 4B) (*11*).

Electrical properties of PEDOT:PSS films

In addition to the mechanical properties, the $NaClO_4$ ductilization also affects the electrical properties of a-EG/PEDOT:PSS. As shown in Fig. 5A, the conductivity of a-EG/PEDOT:PSS films is 775 S cm^{-1} and decreases to 538 S cm^{-1} after the ductilization with the aqueous

Table 1. The PEDOT-to-PSS mass ratio, mechanical properties, and conductivity of ductilized PEDOT:PSS films.

Samples	Elongation at break (%)	Young's modulus (MPa)	Tensile strength (MPa)	PEDOT-to-PSS ratio	Conductivity (S cm^{-1})
$NaClO_4$/a-EG/PEDOT:PSS	53.2	42.9	21.8	0.54	538
$NaClO_4$/p-MSA/ PEDOT:PSS	38.2	60.2	20.6	0.60	1006
$NaClO_4$/p-EG/PEDOT:PSS	36.2	61.2	20.6	0.72	601
$NaClO_4$/p-FA/PEDOT:PSS	35.5	71.0	20.8	0.72	787
NaCl/a-EG/PEDOT:PSS	48.3	89.7	23.2	–	412
NH_4Cl/a-EG/PEDOT:PSS	41.9	107.7	24.2	–	367
$CuCl_2$/a-EG/PEDOT:PSS	32.4	122.9	21.4	–	565

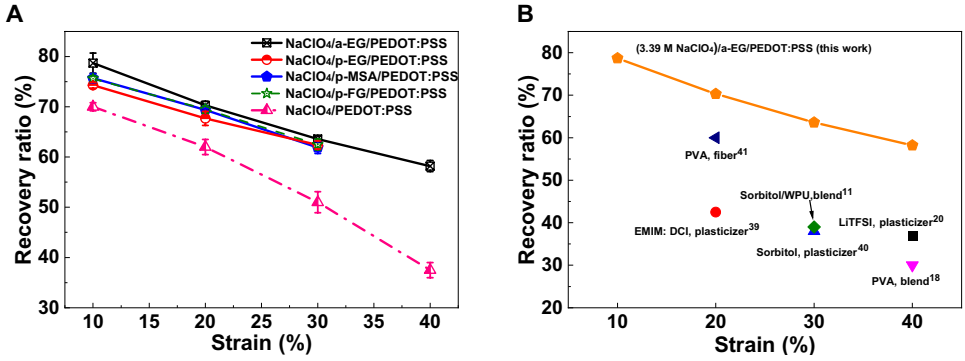

Fig. 4. Elasticity. (**A**) The recovery ratios of PEDOT:PSS films by different treatments at various tensile strains. The error bars represent the SD. (**B**) Comparison of the elasticity with other free-standing PEDOT:PSS plasticized with chemical agents or blending with soft polymers reported in literature (*11*, *18*, *20*, *36*–*38*).

solution of 3.39 M $NaClO_4$. The conductivity of $NaClO_4$/a-EG/PEDOT:PSS films decreases with the increasing $NaClO_4$ concentration. The $NaClO_4$ ductilization only slightly affects the sheet resistance but increases the thickness of the polymer films (fig. S21). The decrease in the conductivity arises from the presence of $NaClO_4$ in the PEDOT:PSS films. The $NaClO_4$ ductilization hardly changes the intrinsic conductivity of a-EG/PEDOT:PSS. This suggests that the ductilization hardly affects the PEDOT networks and the π-π stacking. Hence, the conductivity of the ductilized PEDOT:PSS films is determined primarily by the secondary doping. Among the ductilized PEDOT:PSS films, $NaClO_4$/p-MSA/PEDOT:PSS exhibits the highest conductivity of >1000 S cm^{-1} (Table 1).

The ductilized PEDOT:PSS films show a resistance insensitive to the tensile strain (Fig. 5B). For example, the resistance of $NaClO_4$/a-EG/PEDOT:PSS at the strain of 50% increases only to 1.2 times of its original resistance. This resistance variation with the strain is much less than that caused by the strain-induced geometric effect. For example, the R/R_0 values by experiments are 0.98, 1.01, and 1.05 at the tensile strains of 10, 20, and 30%, respectively, while they are 1.18, 1.36 and 1.56, respectively, by the simulation with the strain-induced geometric effect (*19*). A detailed description of the geometric effect is provided in the note of fig. S22. This difference suggests the orientation of the PEDOT chains during the tensile test, which facilitates the charge transport (*20*, *39*). This indicates that the PEDOT chains can be readily oriented by the stress because of the reduction of the interaction between PEDOT and PSS by $NaClO_4$. The ductile $NaClO_4$/p-EG/PEDOT:PSS, $NaClO_4$/p-MSA/PEDOT:PSS, and $NaClO_4$/p-FA/PEDOT:PSS films also exhibit small resistance variations with the tensile strain, notably lower than that by the strain-induced geometric effect (fig. S22).

The resistance variations of $NaClO_4$/a-EG/PEDOT:PSS films during the cyclic tensile tests are presented in Fig. 5C. The resistance slightly decreases by only ~2% in the cycles with the maximum strain of 10%, and the resistance variation is ~6% in the cycles with the maximum strain of 30%. As shown in Fig. 5D, the resistance variation is very small during the cyclic tests. These results suggest that there may be two factors affecting the resistance of the ductilized PEDOT:PSS films. One is the resistance increase due to the strain-induced geometric effect, and another is the resistance decrease arising from the orientation of the PEDOT chains or aggregates under strain.

Strain-insensitive resistance is required for stretchable electrodes. However, the resistance of all conductive materials should increase under tensile strain as a result of the extension along the longitudinal direction and the shrinkage of the transverse area. If the charge transport mechanism is charge tunneling, then the tensile strain can induce notable resistance variations, such as polymer composites with conductive fillers (*40*). Table S2 lists the resistance variations of some representative stretchable conductors under strain. The $NaClO_4$/a-EG/PEDOT:PSS films show the lowest resistance variation among the stretchable conducting polymers.

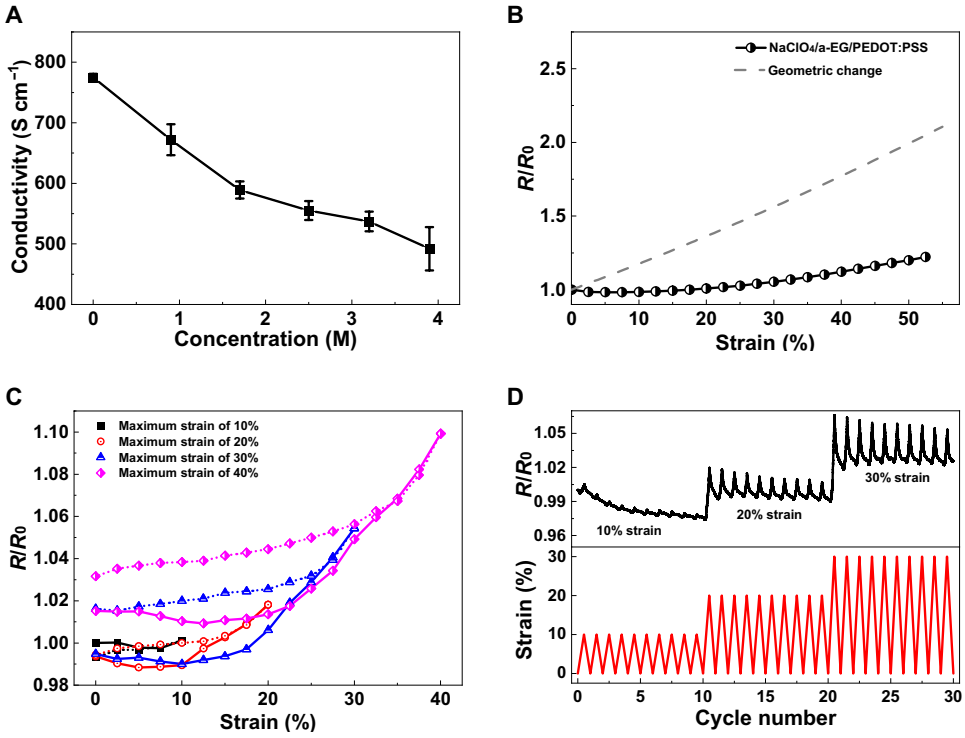

Fig. 5. Electrical properties of PEDOT:PSS films. (**A**) Variations of the conductivity of $NaClO_4$/a-EG/PEDOT:PSS films with the $NaClO_4$ concentration of the ductilization. The error bars represent the SD. (**B**) Variations of the resistance of a $NaClO_4$/a-EG/PEDOT:PSS film with the tensile strain. The dashed curve is the simulation in terms of the strain-induced changes in the length and cross-sectional area of the sample and assumption that the strain does not affect the conductivity. (**C** and **D**) Variations of the resistance of a $NaClO_4$/a-EG/PEDOT:PSS film during cyclic tensile tests. The solid and dotted lines present the stretching and releasing processes, respectively. The $NaClO_4$ concentration of the solution for the ductilization was 3.39 M.

Assuming that the geometry of the $NaClO_4$/a-EG/PEDOT:PSS films uniformly changes under strain, their conductivities under strain were calculated in terms of the resistance. As shown in fig. S23, the conductivity of the $NaClO_4$/a-EG/PEDOT:PSS films increases with the strain. It is 538 S cm^{-1} in the relaxed state and increases to 902 S cm^{-1} at the fracture strain. These values are 1006 and 1321 S cm^{-1}, respectively, for $NaClO_4$/p-MSA/PEDOT:PSS. The increase in the conductivity arises from the orientation of the PEDOT chains induced by the stress.

Mechanisms for the ductilization of PEDOT:PSS

$NaClO_4$/a-EG/PEDOT:PSS films in the relaxed state and at a strain of 30% were studied by the AFM phase microscopy (Fig. 6, A and B). The AFM phase image indicates a uniform structure for the film in the relaxed state. The AFM phase image notably changes when the film is under the strain of 30%. Some grains elongate along the stretching direction. Similar changes were also observed in the AFM topological images (fig. S24). The change in the polymer chain orientation was also observed by the polarized UV-visible (UV-Vis) absorption spectroscopy. As shown in fig. S25, the $NaClO_4$/a-EG/PEDOT:PSS film is isotropic before the tensile testing and becomes anisotropic under a tensile strain. The absorption with the polarized light along the tensile direction becomes much higher than that perpendicular to the tensile direction. The dichroic ratio of absorption along the two directions at 700 nm becomes 4.8 under the strain of 50%. These results evidence the orientation of PEDOT chains or aggregates under stress as illustrated in Fig. 6C (*20*, *39*, *41*).

The tensile strain can also affect the Raman spectra of PEDOT:PSS. The Raman band at 1435 cm^{-1} shifts red to 1433 cm^{-1} after the $NaClO_4$/EG/PEDOT:PSS film is stretched to the strain of 30% and becomes narrower (Fig. 6D and fig. S26). This Raman band is sensitive to the PEDOT chain conformation and the doping level. Because the mechanical strain should not affect the doping level of PEDOT:PSS, the change in this Raman band implies that the conformation of PEDOT becomes more linear under stress (*42*–*44*). It is understandable that mechanical stress can induce the orientation of polymer chains and thus their conformation (*20*, *41*). The linear conformation of PEDOT chains can facilitate the charge transport and thus increase the conductivity.

The salt effect can be understood in terms of the interaction among the ions. Because both the salts and PEDOT:PSS are made of ions, the ions (A^+ and B^-) of a salt can associate with the polyions of PEDOT:PSS as $PEDOT^+PSS^- + A^+ + B^- \leftrightarrow PEDOT^+B^- + A^+PSS^-$ (*45*).

This kind of ion associations can lower the interchain interaction of nonconductive polyelectrolyte complexes (*46*). As a result, the deformation and slippage of the polymer chains under stress become easier. This can lower the tensile strength and Young's modulus of the polyelectrolytes because the nonconductive polyelectrolyte complexes are composed of saturated polycations and polyanions, and there is no π-π stacking among the polymer chains (*47*, *48*). Thus, a salt treatment of nonconductive polyelectrolytes can induce the plasticization instead of the ductilization. This becomes different for PEDOT:PSS made of conjugated $PEDOT^+$ and saturated PSS^-. Because $PEDOT^+$ is much more rigid than PSS^- and there is π-π

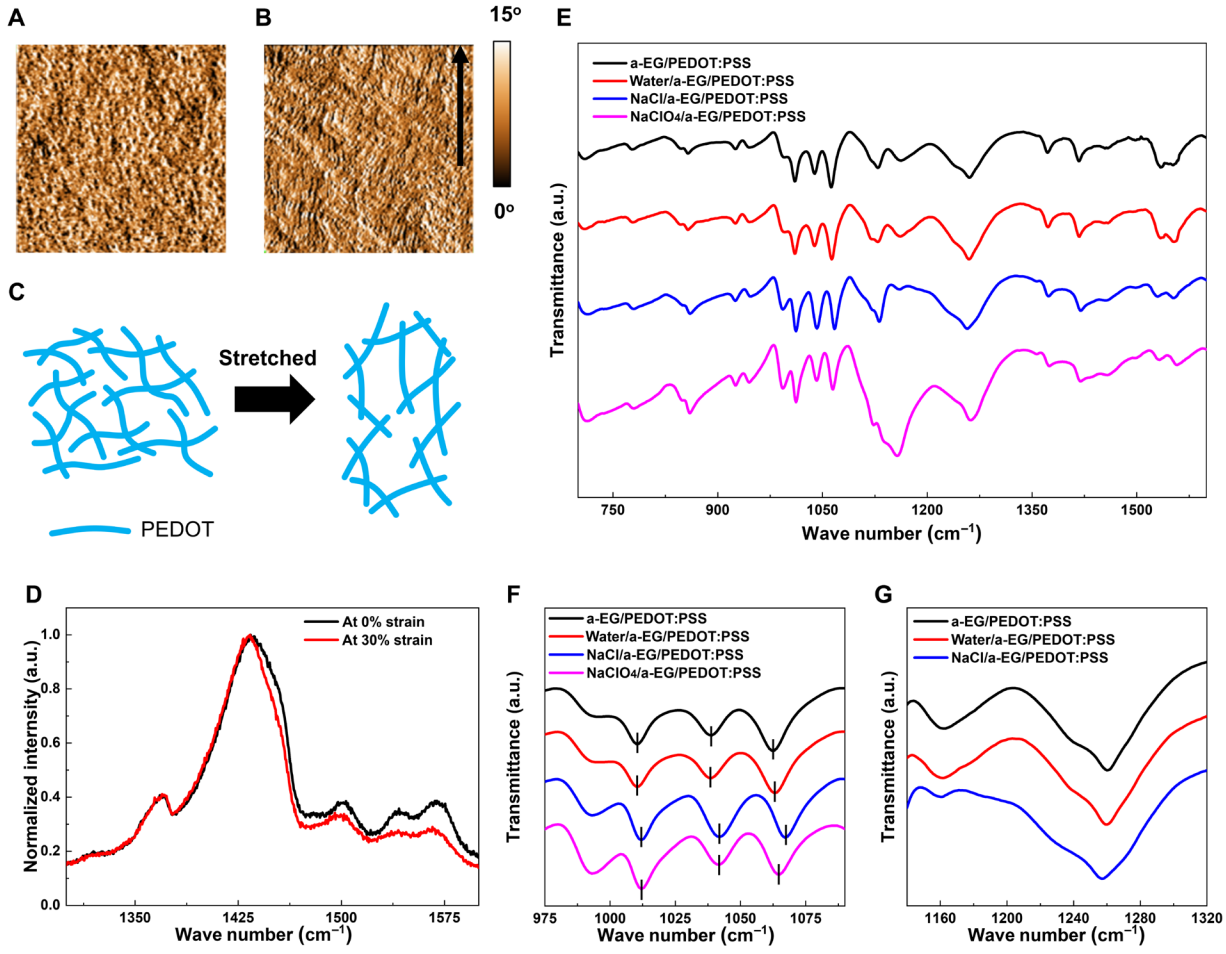

Fig. 6. AFM images and vibrational spectra. AFM phase images of $NaClO_4$/a-EG/PEDOT:PSS films at the strains of (**A**) 0% and (**B**) 30%. The image size is 2 μm by 2 μm, and the arrow specifies the stretching direction. (**C**) Schematic illustrations of the orientation of polymer chains under stress. (**D**) Raman spectra of $NaClO_4$/a-EG/PEDOT:PSS films at the strains of 0 and 30%. FTIR spectra of a-EG/PEDOT:PSS films by various treatments within the range of (**E**) 675 to 1600 cm^{-1}, (**F**) 975 to 1090 cm^{-1}, and (**G**) 1140 to 1320 cm^{-1}.

stacking among the $PEDOT^+$ chains, the mechanical properties of PEDOT:PSS are dominated by the PEDOT networks. As evidenced by the conductivity, the ductilization of PEDOT:PSS with a salt does not affect the $PEDOT^+$ networks. Hence, the tensile strength hardly changes since it is related to the breakdown of the PEDOT networks.

The interaction between the polyions of PEDOT:PSS and the ions of $NaClO_4$ or NaCl was studied by Fourier transform infrared (FTIR) spectroscopy (Fig. 6, E to G, and figs. S27 to S29). The main IR bands of PEDOT:PSS are summarized in table S3. Because the control study to treat a-EG/PEDOT:PSS with water does not remarkably change the IR bands, the change in the IR bands after the ductilization of a-EG/PEDOT:PSS with a salt suggests the interaction between the ions of the salts and PEDOT:PSS. The bands at 1000 to 1200 cm^{-1} are sensitive to the associated cations of PSS^- (*49*–*51*). The symmetric SO_3^- stretching band shifts from 1039 to 1042 cm^{-1} after the ductilization of a-EG/PEDOT:PSS with $NaClO_4$ or NaCl (Fig. 6F). In addition, the asymmetric SO_3^- stretching band at 1162 cm^{-1} becomes weaker, while its adjacent band becomes broader after the NaCl treatment (Fig. 6G and fig. S28). These changes can be ascribed to the removal of the degeneracy of the SO_3^- asymmetric vibration, thus causing the splitting (*49*, *50*). The C—O—C stretching band of PEDOT is also indicative of the interaction between PEDOT:PSS and a salt (*52*, *53*). It appears at 1063 cm^{-1} for a-EG/PEDOT:PSS and shifts to 1065 or 1067 cm^{-1} after the ductilization with $NaClO_4$ or NaCl (Fig. 6F). The C—S vibration band of the thiophene ring also shifts from 857 to 860 cm^{-1} after the ductilization (fig. S29).

Figure 7A schematically illustrates the conformation of PEDOT and PSS chains and the Coulomb attraction between $PEDOT^+$ and PSS^- of a-EG/PEDOT:PSS. The Coulomb attraction is so strong that the slippage of the polymer chains is very difficult under stress. Hence, a-EG/PEDOT:PSS is very brittle. As shown in the Fig. 7B, the presence of a salt can greatly reduce the Coulomb attraction between $PEDOT^+$ and PSS^- as a result of the association of the ions of the salt with $PEDOT^+$ and PSS^-. Hence, the slippage of the polymer chains can occur under stress. However, when a $PEDOT^+$ or PSS^- chain slips to a new site, it has almost the same Coulomb attraction to the other polymer chains. In addition, the conductive PEDOT networks are preserved via the π-π stacking (Fig. 7B). When a stress is applied to the ductilized a-EG/PEDOT:PSS film, the slippage and deformation of the polymer chains become easy because of the weakened Coulomb attraction between $PEDOT^+$ and PSS^-. The PEDOT chains can also orient along the tensile structure (Fig. 7C). This can greatly

lower the Young's modulus since the Young's modulus of a polymer depends on the interchain interaction. Because the PEDOT networks are formed via π-π stacking and are not affected by the salts, the breakdown of the PEDOT networks is not affected by the salt, and the tensile strength thus hardly changes.

This ductilization mechanism is evidenced by the different ductilizations of PEDOT:PSS by different salts. The small cations and anions of a salt must dissociate, $A^+B^- \rightarrow A^+ + B^-$, for their association with the polyions of PEDOT:PSS. Hence, the lattice energy of the salts should be related to the ductilization. The lattice energies are 641, 708, 790, and 2824 kJ mol^{-1} for $NaClO_4$, NH_4Cl, NaCl, and $CuCl_2$, respectively (*54*). Among them, $NaClO_4$ has the lowest lattice energy and gives rise to the highest ductilization, while $CuCl_2$ has the highest lattice energy and leads to the lowest ductilization. In addition, the hydration of the small cations and anions can facilitate their dissociation. This indicates that the hydration energy of the ions can affect the ductlization as well. The hydration energies are −365 and −285 kJ mol^{-1} for Na^+ and NH_4^+, respectively (*55*). This can be the reason that NaCl can give rise to higher ductilization of PEDOT:PSS than NH_4Cl, although NaCl has a higher lattice energy than NH_4Cl. The hydration energy of ClO_4^- is −430 kJ mol^{-1}, higher than that (−340 kJ mol^{-1}) of Cl^- (*55*). Thus, the salt crystallization does not occur at a low RH for a-EG/PEDOT:PSS ductilized by $NaClO_4$, while it takes place for that by NaCl or NH_4Cl.

This ductilization mechanism is also consistent with the other experimental results. The Young's modulus depends on the interchain interaction, and the interchain interaction of ductilized a-EG/PEDOT:PSS is related to the amount of the salt ions in PEDOT:PSS. Thus, the Young's modulus of a-EG/PEDOT:PSS decreases with the increasing $NaClO_4$ concentration. At high $NaClO_4$ concentration, the stress-strain curve of a-EG/PEDOT:PSS becomes linear. Similar linear relationship was also observed on nonconductive polyelectrolytes with a salt (*45*–*48*). This is probably related to the slippage of the polycations or polyanions because the polymer chain slippage basically does not affect the Coulomb attraction between the polycations and polyanions. Thus, the stress-strain behavior is saliently different from the plastic deformation of general polymers. Because the conjugated PEDOT chains form networks via π-π stacking, the ductilized a-EG/PEDOT:PSS can exhibit high conductivity. The conductivity even increases at high tensile strain, arising from the orientation of the PEDOT chains along the tensile direction.

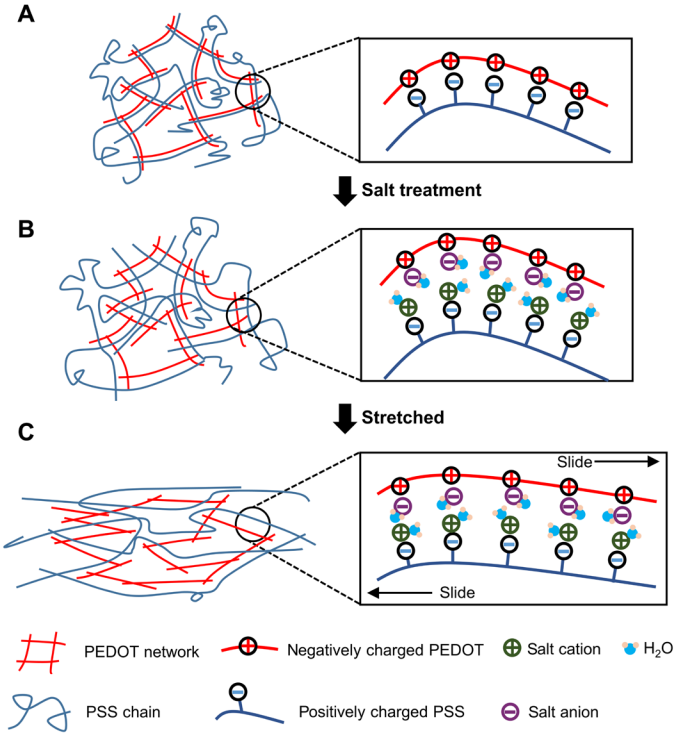

Fig. 7. Schematic illustrations of the mechanism for salt-induced ductilization. (**A**) The conformation (left) and Coulomb attraction (right) between PEDOT and PSS at the absence of salt. The conformation of PEDOT and PSS chains and their interaction with salt ions (**B**) at rest and (**C**) under a tensile stress for a-EG/PEDOT:PSS ductilized with a salt.

DISCUSSION

Both high mechanical ductility and high tensile strength are essential mechanical properties. Polymers with high ductility can endure large mechanical deformation, while high tensile strength makes them resistant to fracture under high mechanical stress. Mechanical torment is ubiquitous when electronic devices function in real situations. It increases the damage risk of devices, particularly for stretchable constituents, because their strength is always sacrificed to achieve high elongation at break. The enhancement in the tensile strength makes them more tolerant to mechanical force and energy that can be applied unexpectedly during handling, transferring, and operating. Thus, it is of great benefit to the durability and stability of stretchable conductors under practical conditions.

However, the popular methods to improve the elongation at break of polymers saliently lower the tensile strength, such as plasticization and blending with elastomers. In this work, we observed the ductilization of a polymer by salts. Treating PEDOT:PSS by a salt such as $NaClO_4$ can greatly increase the elongation at break while hardly affecting its tensile strength, that is, they can ductilize PEDOT:PSS. The ductilized a-EG/PEDOT:PSS film can exhibit a conductivity of 538 S cm^{-1}, an elongation at break of 53.2%, and a tensile strength of 21.8 MPa. In addition, the ductilized polymer films can exhibit a resistance insensitive to the tensile strain. It can serve as the stretchable interconnect and function well under mechanical stress owing to its high tensile strength. This is demonstrated in fig. S30. The ductilization method by the salt treatment is facial and effective, which shows great potential to be developed for many important applications such as electronic textiles and electromagnetic shielding.

The salt-induced ductilization of PEDOT:PSS can be attributed to the weakening of the Coulombic interaction between $PEDOT^+$ and PSS^- by the salt ions. However, this hardly affects the PEDOT networks in PEDOT:PSS. Although the phase AFM images indicate that the salt ductilization can also affect the interface between the PEDOT-rich grains and the PSS-rich grains of PEDOT:PSS, this change in the interface may not be the main reason for the ductilization of PEDOT:PSS because secondary doping also noticeably affects the interface between the two types of the grains but hardly affects the tensile strength and the elongation at break. This ductiliztion strategy for PEDOT:PSS can be applicable for other polymers with hard and soft components, of which the hard component can form networks, and the interaction between the hard and soft components can be varied by a chemical such as salt. For example, other ICPs with a polyelectrolyte as the counter ion can be ductilized by this way.

The ductilization mechanism of PEDOT:PSS is different from that of metals. The ductilization of metals is due to the control of the interfacial energy between nanocrystalline metal particles or grain and the matrix (*1*–*4*). The nanocrystalline metal can have high strength but low ductility, while the matrix can have high ductility but limited strength. Controlling the interface between the nanocrystalline structure and the matrix can effectively help the energy transfer from the matrix to the nanocrystalline structure to achieve high strength and high ductility. However, there are some similarities for the ductilization of these two types of materials. There are two phases for the metals, while there are two components with different mechanical properties for the polymers. The ductilization of metal is related to the interfacial interaction of the two phases, while the ductilization of polymers arises from the weakening of the interaction between the hard and soft components.

MATERIALS AND METHODS

Materials

PEDOT:PSS (Clevios PH1000) was purchased from Heraeus. The mass ratio of PEDOT to PSS is 1:2.5, and the solid content of Clevios PH1000 is between 1.0 and 1.3 wt %. EG (ReagentPlus; >99%), FA (ACS reagent; >96%), MSA (~99.5%), copper(II) chloride ($CuCl_2$; 97%), and PSSH solution (18 wt % PSSH in water, molecular weight of ~75,000) were supplied by Sigma-Aldrich. Sodium chloride (NaCl; AR grade) and anhydrous sodium perchloride ($NaClO_4$; ACS reagent; 98.0 to 102.0%) were obtained from Schedelco Pte. Ltd. and Alfa Aesar, respectively. All chemicals were used as received.

Fabrication of free-standing pristine PEDOT:PSS films

Glass substrates were cleaned successively with detergent, deionized water (DI water), acetone, and isopropyl alcohol under ultrasonication for 15 min. The as-received PEDOT:PSS dispersion was dropcasted on the glass substrates and then dried at 60°C on a hotplate for about 1 hour. The PEDOT:PSS films were further annealed at 160°C for 10 min.

Fabrication of free-standing a-EG/PEDOT:PSS films

EG (5 wt %) was added into the PEDOT:PSS aqueous dispersion. It was then dropcasted on glass substrate and dried at 120°C on a hotplate for 15 min. After cooling down to room temperature for 10 min, it was annealed at 160°C for 10 min. These films are represented by a-EG/PEDOT:PSS.

Posttreatment of PEDOT:PSS

A PEDOT:PSS film posttreated with EG was prepared by droping EG on an as-prepared pristine PEDOT:PSS film and then annealed at 120°C for 20 min. These films are called p-EG/PEDOT:PSS.

A PEDOT:PSS posttreated with MSA was prepared by dropping 8 M MSA aqueous solution on an as-prepared pristine PEDOT:PSS film and then annealed at 160°C for 10 min. After cooling down to room temperature, DI water was dropped onto the film for 30 s, and the DI water was then removed by spin coating. This rinsing process was repeated three times. The sample was subsequently annealed at 160°C for 10 min. The posttreatment with FA was carried out at 140°C for 5 min. The annealing temperatures for different acids are determined on the basis of optimum conditions reported in literature (*32*, *56*).

Ductilization

A salt solution was dropped onto a PEDOT:PSS film treated with an organic compound. It was then sealed at room temperature for 12 hours. The salt solution was then removed from the PEDOT:PSS film by spin coating. The ductilized PEDOT:PSS film was dried at ambient conditions for at least 6 hours before further measurements.

Measurements of PEDOT:PSS films at different humidities

The PEDOT:PSS film at 25% RH represents the sample stored at 25% for at least 1 hour before further measurements. The PEDOT:PSS film at 85% RH (reversion) represents that the sample was stored for at least 1 hour at 25% RH and then moved to 85% RH for at least 12 hours before further measurements.

Characterizations and measurements

The conductivities of free-standing PEDOT:PSS thin films were measured by the four-probe method. The thicknesses were determined using an Alpha 500 step profiler. The electrical resistance variations during tensile testing were measured by the two-probe method with copper wires and silver paste applied as the contacts. Mechanical properties were tested using an Instron 3345 machine with a load cell of 1 kN. The dimensions of each sample were 1.5 mm by 7 mm, and the contact area with the fixture was protected by hard materials from the clamping force. The strain rate was 7.1% min^{-1} unless otherwise specified.

The Raman spectra were taken on the samples on glass substrate with a LabRam HR 800 Raman spectrometer by Horiba Jobin-Yvon with the Ar^+ laser of 514.5 nm. AFM images were obtained with a MultiMode AFM (NanoScope IV) by Veeco with the tapping mode. The AFM samples were on glass substrate, and a sample under strain was fixed by tape. Attenuated total reflection FTIR (ATR-FTIR) spectra were taken using a PerkinElmer Frontier mid-infrared instrument with a diamond-attenuated total reflectance crystal. The samples for ATR-FTIR were free-standing films peeled from the glass substrate, and they had a thickness of 10 to 20 μm. The XRD patterns were obtained on the samples on single crystal silicon substrate with a Bruker D8 ADVANCE XRD instrument. The UV-Vis spectra were acquired from the samples on quartz substrate using a UV-1800 spectrophotometer by Shimadzu. SEM images and EDX element mapping were taken using a Zeiss GeminiSEM 300 Field Emission SEM equipped with Ultim Max and AZtecLive by Oxford Instruments NanoAnalysis. Optical microscopy images were obtained using a Nikon Eclipse LV100ND.

SUPPLEMENTARY MATERIALS

Supplementary material for this article is available at https://science.org/doi/10.1126/sciadv.abq8160

REFERENCES AND NOTES

1. I. V. Okulov, I. V. Soldatov, M. F. Sarmanova, I. Kaban, T. Gemming, K. Edström, J. Eckert, Flash Joule heating for ductilization of metallic glasses. *Nat. Commun.* **6**, 7932 (2015).
2. Y. M. Wang, T. Voisin, J. T. McKeown, J. Ye, N. P. Calta, Z. Li, Z. Zeng, Y. Zhang, W. Chen, T. T. Roehling, R. T. Ott, M. K. Santala, P. J. Depond, M. J. Matthews, A. V. Hamza, T. Zhu, Additively manufactured hierarchical stainless steels with high strength and ductility. *Nat. Mater.* **17**, 63–71 (2018).
3. A. Khalajhedayati, Z. Pan, T. J. Rupert, Manipulating the interfacial structure of nanomaterials to achieve a unique combination of strength and ductility. *Nat. Commun.* **7**, 10802 (2016).
4. S. Sandlöbes, Z. Pei, M. Friák, L.-F. Zhu, F. Wang, S. Zaefferer, D. Raabe, J. Neugebauer, Ductility improvement of Mg alloys by solid solution: Ab initio modeling, synthesis and mechanical properties. *Acta Mater.* **70**, 92–104 (2014).

5. Y. Wang, Q. Fu, Q. Li, G. Zhang, K. Shen, Y. Z. Wang, Ductile–brittle-transition phenomenon in polypropylene/ethylene-propylene-diene rubber blends obtained by dynamic packing injection molding: A new understanding of the rubber-toughening mechanism. *J. Polym. Sci. Part B: Polym. Phys.* **40**, 2086–2097 (2002).
6. C. J. Chou, K. Vijayan, D. Kirby, A. Hiltner, E. Baer, Ductile-to-brittle transition of rubber-modified polypropylene. *J. Mater. Sci.* **23**, 2533–2545 (1988).
7. G. Wypych, Effect of plasticizers on properties of plasticized materials, in *Handbook of Plasticizers*, G. Wypych, Ed. (ChemTec Publishing, 2017), chap. 10, pp. 210–214.
8. A. X. Chen, A. T. Kleinschmidt, K. Choudhary, D. J. Lipomi, Beyond stretchability: Strength, toughness, and elastic range in semiconducting polymers. *Chem. Mater.* **32**, 7582–7601 (2020).
9. D. Lee, S. H. Song, J. Hwang, S. H. Jin, K. H. Park, B. H. Kim, S. H. Hong, S. Jeon, Enhanced mechanical properties of epoxy nanocomposites by mixing noncovalently functionalized boron nitride nanoflakes. *Small* **9**, 2602–2610 (2013).
10. M. Morits, T. Verho, J. Sorvari, V. Liljeström, M. A. Kostiainen, A. H. Gröschel, O. Ikkala, Toughness and fracture properties in nacre-mimetic clay/polymer nanocomposites. *Adv. Funct. Mater.* **27**, 1605378 (2017).
11. L. Zhang, K. S. Kumar, H. He, C. J. Cai, X. He, H. Gao, S. Yue, C. Li, R. C. S. Seet, H. Ren, J. Ouyang, Fully organic compliant dry electrodes self-adhesive to skin for long-term motion-robust epidermal biopotential monitoring. *Nat. Commun.* **11**, 4683 (2020).
12. T. A. Skotheim, J. Reynolds, *Handbook of Conducting Polymers* (CRC Press, 1986).
13. V. R. Feig, H. Tran, M. Lee, Z. Bao, Mechanically tunable conductive interpenetrating network hydrogels that mimic the elastic moduli of biological tissue. *Nat. Commun.* **9**, 2740 (2018).
14. H. Yuk, B. Lu, X. Zhao, Hydrogel bioelectronics. *Chem. Soc. Rev.* **48**, 1642–1667 (2019).
15. V. Kalidasan, X. Yang, Z. Xiong, R. R. Li, H. Yao, H. Godaba, S. Obuobi, P. Singh, X. Guan, X. Tian, S. A. Kurt, Z. Li, D. Mukherjee, R. Rajarethinam, C. S. Chong, J. W. Wang, P. L. R. Ee, W. Loke, B. C. K. Tee, J. Ouyang, C. J. Charles, J. S. Ho, Wirelessly operated bioelectronic sutures for the monitoring of deep surgical wounds. *Nat. Biomed. Eng.* **5**, 1217–1227 (2021).
16. P. Li, D. Du, L. Guo, Y. Guo, J. Ouyang, Stretchable and conductive polymer films for high-performance electromagnetic interference shielding. *J. Mater. Chem. C* **4**, 6525–6532 (2016).
17. J. Chen, J. Liu, T. Thundat, H. Zeng, Polypyrrole-doped conductive supramolecular elastomer with stretchability, rapid self-healing, and adhesive property for flexible electronic sensors. *ACS Appl. Mater. Interfaces* **11**, 18720–18729 (2019).
18. P. Li, K. Sun, J. Ouyang, Stretchable and conductive polymer films prepared by solution blending. *ACS Appl. Mater. Interfaces* **7**, 18415–18423 (2015).
19. H. He, L. Zhang, X. Guan, H. Cheng, X. Liu, S. Yu, J. Wei, J. Ouyang, Biocompatible conductive polymers with high conductivity and high stretchability. *ACS Appl. Mater. Interfaces* **11**, 26185–26193 (2019).
20. Y. Wang, C. Zhu, R. Pfattner, H. Yan, L. Jin, S. Chen, F. Molina-Lopez, F. Lissel, J. Liu, N. I. Rabiah, Z. Chen, J. W. Chung, C. Linder, M. F. Toney, B. Murmann, Z. Bao, A highly stretchable, transparent, and conductive polymer. *Sci. Adv.* **3**, e1602076 (2017).
21. S. T. Dubas, J. B. Schlenoff, Swelling and smoothing of polyelectrolyte multilayers by salt. *Langmuir* **17**, 7725–7727 (2001).
22. J. Rivnayu, S. Inal, B. A. Collins, M. Sessolo, E. Stavrinidou, X. Strakosas, C. Tassone, D. M. Delongchamp, G. G. Malliaras, Structural control of mixed ionic and electronic transport in conducting polymers. *Nat. Commun.* **7**, 11287 (2016).
23. M. Modarresi, A. Mehandzhiyski, M. Fahlman, K. Tybrandt, I. Zozoulenko, Microscopic understanding of the granular structure and the swelling of PEDOT: PSS. *Macromolecules* **53**, 6267–6278 (2020).
24. H. Shi, C. Liu, Q. Jiang, J. Xu, Effective approaches to improve the electrical conductivity of PEDOT:PSS: A review. *Adv. Electron. Mater.* **1**, 1500017 (2015).
25. C. M. Palumbiny, F. Liu, T. P. Russell, A. Hexemer, C. Wang, P. Müller-Buschbaum, The crystallization of PEDOT:PSS polymeric electrodes probed in situ during printing. *Adv. Mater.* **27**, 3391–3397 (2015).
26. J. Ouyang, "Secondary doping" methods to significantly enhance the conductivity of pedot:pss for its application as transparent electrode of optoelectronic devices. *Displays* **34**, 423–436 (2013).
27. S. N. Magonov, V. Elings, M. H. Whangbo, Phase imaging and stiffness in tapping-mode atomic force microscopy. *Surf. Sci.* **375**, L385–L391 (1997).
28. Y. Wang, R. Song, Y. Li, J. Shen, Understanding tapping-mode atomic force microscopy data on the surface of soft block copolymers. *Surf. Sci.* **530**, 136–148 (2003).
29. N. Kim, S. Kee, S. H. Lee, B. H. Lee, Y. H. Kahng, Y. R. Jo, B. J. Kim, K. Lee, Highly conductive PEDOT:PSS nanofibrils induced by solution-processed crystallization. *Adv. Mater.* **26**, 2268–2272 (2014).
30. D. Li, L. Zhou, X. Wang, L. He, Y. Xiong, Effect of crystallinity of polyethylene with different densities on breakdown strength and conductance property. *Materials* **12**, 1746 (2019).
31. H. W. Starkweather Jr., G. E. Moore, J. E. Hansen, T. M. Roder, R. E. Brooks, Effect of crystallinity on the properties of nylons. *J. Polym. Sci.* **21**, 189–204 (1956).
32. J. Ouyang, Solution-processed PEDOT:PSS films with conductivities as indium tin oxide through a treatment with mild and weak organic acids. *ACS Appl. Mater. Interfaces* **5**, 13082–13088 (2013).
33. Y. H. Kim, C. Sachse, M. L. Machala, C. May, L. Müller-Meskamp, K. Leo, Highly conductive PEDOT:PSS electrode with optimized solvent and thermal post-treatment for ITO-free organic solar cells. *Adv. Funct. Mater.* **21**, 1076–1081 (2011).
34. J. S. Yeo, J. M. Yun, D. Y. Kim, S. Park, S. S. Kim, M. H. Yoon, T. W. Kim, S. I. Na, Significant vertical phase separation in solvent-vapor-annealed poly (3, 4-ethylenedioxythiophene):poly (styrene sulfonate) composite films leading to better conductivity and work function for high-performance indium tin oxide-free optoelectronics. *ACS Appl. Mater. Interfaces* **4**, 2551–2560 (2012).
35. Y. Xia, J. Sun, J. Ouyang, Solution-processed metallic conducting polymer films as transparent electrode of optoelectronic devices. *Adv. Mater.* **24**, 2436–2440 (2012).
36. S. Kee, H. Kim, S. H. K. Paleti, A. El Labban, M. Neophytou, A. H. Emwas, H. N. Alshareef, D. Baran, Highly stretchable and air-stable PEDOT: PSS/ionic liquid composites for efficient organic thermoelectrics. *Chem. Mater.* **31**, 3519–3526 (2019).
37. H. He, L. Zhang, S. Yue, S. Yu, J. Wei, J. Ouyang, Enhancement in the mechanical stretchability of PEDOT: PSS films by compounds of multiple hydroxyl groups for their application as transparent stretchable conductors. *Macromolecules* **54**, 1234–1242 (2021).
38. Q. Gao, M. Wang, X. Kang, C. Zhu, M. Ge, Continuous wet-spinning of flexible and water-stable conductive PEDOT: PSS/PVA composite fibers for wearable sensors. *Compos. Commun.* **17**, 134–140 (2020).
39. Y. Kim, H. Noh, B. D. Paulsen, J. Kim, I. Y. Jo, H. J. Ahn, J. Rivnay, M. H. Yoon, Strain-engineering induced anisotropic crystallite orientation and maximized carrier mobility for high-performance microfiber-based organic bioelectronic devices. *Adv. Mater.* **33**, 2007550 (2021).
40. H. Joo, D. Jung, S. H. Sunwoo, J. H. Koo, D. H. Kim, Material design and fabrication strategies for stretchable metallic nanocomposites. *Small* **16**, 1906270 (2020).
41. D. Lipomi, J. A. Lee, M. Vosgueritchian, B. C. K. Tee, J. A. Bolander, Z. Bao, Electronic properties of transparent conductive films of PEDOT:PSS on stretchable substrates. *Chem. Mater.* **24**, 373–382 (2012).
42. J. Ouyang, Q. Xu, C. W. Chu, Y. Yang, G. Li, J. Shinar, On the mechanism of conductivity enhancement in poly(3,4-ethylenedioxythiophene):poly(styrene sulfonate) film through solvent treatment. *Polymer* **45**, 8443–8450 (2004).
43. A. Hu, L. Tan, X. Hu, L. Hu, Q. Ai, X. Meng, L. Chen, Y. Chen, Crystallization and conformation engineering of solution-processed polymer transparent electrodes with high conductivity. *J. Mater. Chem. C* **5**, 382–389 (2017).
44. A. K. K. Kyaw, T. A. Yemata, X. Wang, S. L. Lim, W. S. Chin, K. Hippalgaonkar, J. Xu, Enhanced thermoelectric performance of PEDOT:PSS films by sequential post-treatment with formamide. *Macromol. Mater. Eng.* **303**, 1700429 (2018).
45. P. Schaaf, J. B. Schlenoff, Saloplastics: Processing compact polyelectrolyte complexes. *Adv. Mater.* **27**, 2420–2432 (2015).
46. R. F. Shamoun, H. H. Hariri, R. A. Ghostine, J. B. Schlenoff, Thermal transformations in extruded saloplastic polyelectrolyte complexes. *Macromolecules* **45**, 9759–9767 (2012).
47. H. H. Hariri, J. B. Schelenoff, Saloplastic macroporous polyelectrolyte complexes: Cartilage mimics. *Macromolecules* **43**, 8656–8663 (2010).
48. R. F. Shamoun, A. Reisch, J. B. Schlenoff, Extruded saloplastic polyelectrolyte complexes. *Adv. Funct. Mater.* **22**, 1923–1931 (2012).
49. J. Fitzgerald, R. Weiss, Cation-anion and cation-cation interactions in sulfonated polystyrene ionomers: Spectroscopic studies of the effects of solvents, in *Coulombic Interactions in Macromolecular Systems*, A. Eisenberg, F. E. Bailey, Eds. (ACS, 1986), chap. 3, pp. 35–53.
50. R. A. Weiss, J. J. Fitzgerald, Effect of solvents on structure and properties of ionomers, in *Structure and Properties of Ionomers*, vol. 198 of *NATO ASI Series (Series C: Mathematical and Physical Science)*, M. Pineri, A. Eisenberg, Eds. (Springer, 1987), pp. 363–365.
51. T. Farhat, G. Yassin, S. T. Dubas, J. B. Schlenoff, Water and ion pairing in polyelectrolyte multilayers. *Langmuir* **15**, 6621–6623 (1999).
52. K. M. Cable, K. A. Mauritz, R. B. Moore, Effects of hydrophilic and hydrophobic counterions on the Coulombic interactions in perfluorosulfonate ionomers. *J. Polym. Sci. B: Polym. Phys.* **33**, 1065–1072 (1995).
53. M. Falk, Infrared spectra of perfluorosulfonated polymer and of water in perfluorosulfonated polymer, in *Perfluorinated Ionomer Membranes*, vol. 180 of *ACS Symposium Series*, A. Eisenberg, H. L. Yeager, Eds. (ACS 1982), pp. 150–155.
54. W. M. Haynes, D. R. Lide, T. J. Bruno, Properties of solids, in *CRC Handbook of Chemistry and Physics,* W. M. Haynes, D. R. Lide, T. J. Bruno, Eds. (CRC Press, 2016), Chapter 12.
55. Y. Marcus, Thermodynamics of solvation of ions. Part 5.- Gibbs free energy of hydration at 298.15 K. *J. Chem. Soc. Faraday Trans.* **87**, 2995–2999 (1991).
56. D. A. Mengistie, M. A. Ibrahem, P. C. Wang, C. W. Chu, Highly conductive PEDOT:PSS treated with formic acid for ITO-free polymer solar cells. *ACS Appl. Mater. Interfaces* **6**, 2292–2299 (2014).

57. M. Feist, Thermal analysis: Basics, applications, and benefit. *ChemTexts* **1**, 8 (2015).
58. R. Ma, B. Kang, S. Cho, M. Choi, S. Baik, Extraordinarily high conductivity of stretchable fibers of polyurethane and silver nanoflowers. *ACS Nano* **9**, 10876–10886 (2015).
59. J. Liang, L. Li, X. Niu, Z. Yu, Q. Pei, Elastomeric polymer light-emitting devices and displays. *Nat. Photonics* **7**, 817–824 (2013).
60. Y. Lu, J. Jiang, S. Yoon, K. S. Kim, J. H. Kim, S. Park, S. H. Kim, L. Piao, High-performance stretchable conductive composite fibers from surface-modified silver nanowires and thermoplastic polyurethane by wet spinning. *ACS Appl. Mater. Interfaces* **10**, 2093–2104 (2018).
61. S. Choi, S. I. Han, D. Jung, H. J. Hwang, C. Lim, S. Bae, O. K. Park, C. M. Tschabrunn, M. Lee, S. Y. Bae, J. W. Yu, J. H. Ryu, S. W. Lee, K. Park, P. M. Kang, W. B. Lee, R. Nezafat, T. Hyeon, D. H. Kim, Highly conductive, stretchable and biocompatible Ag–Au core–sheath nanowire composite for wearable and implantable bioelectronics. *Nat. Nanotechnol.* **13**, 1048–1056 (2018).
62. S. Lee, S. Shin, S. Lee, J. Seo, J. Lee, S. Son, H. J. Cho, H. Algadi, S. Al-Sayari, D. E. Kim, T. Lee, Ag nanowire reinforced highly stretchable conductive fibers for wearable electronics. *Adv. Funct. Mater.* **25**, 3114–3121 (2015).
63. N. Matsuhisa, M. Kaltenbrunner, T. Yokota, H. Jinno, K. Kuribara, T. Sekitani, T. Someya, Printable elastic conductors with a high conductivity for electronic textile applications. *Nat. Commun.* **6**, 7461 (2015).
64. Z. Jiang, O. G. Nayeem, K. Fukuda, S. Ding, H. Jin, T. Yokota, D. Inoue, D. Hashizume, T. Someya, Highly stretchable metallic nanowire networks reinforced by the underlying randomly distributed elastic polymer nanofibers via interfacial adhesion improvement. *Adv. Mater.* **31**, 1903446 (2019).
65. L. Cai, J. Li, P. Luan, H. Dong, D. Zhao, Q. Zhang, X. Zhang, M. Tu, Q. Zeng, W. Zhou, S. Xie, Highly transparent and conductive stretchable conductors based on hierarchical reticulate single-walled carbon nanotube architecture. *Adv. Funct. Mater.* **22**, 5238–5244 (2012).
66. D. J. Lipomi, M. Vosgueritchian, B. C. K. Tee, S. L. Hellstrom, J. A. Lee, C. H. Fox, Z. Bao, Skin-like pressure and strain sensors based on transparent elastic films of carbon nanotubes. *Nat. Nanotechnol.* **6**, 788–792 (2011).
67. G. Chen, R. Rastak, Y. Wang, H. Yan, V. Feig, Y. Liu, Y. Jiang, S. Chen, F. Lian, F. Molina-Lopez, L. Jin, K. Cui, J. W. Chung, E. Pop, C. Linder, Z. Bao, Strain- and strain-rate-invariant conductance in a stretchable and compressible 3D conducting polymer foam. *Matter* **1**, 205–218 (2019).
68. C. Con, B. Cui, Surface nanostructures formed by phase separation of metal salt–polymer nanocomposite film for anti-reflection and super-hydrophobic applications. *Nanoscale Res. Lett.* **12**, 628 (2017).
69. C. Rodriguez-Navarro, L. Linares-Fernandez, E. Doehne, E. Sebastian, Effects of ferrocyanide ions on NaCl crystallization in porous stone. *J. Cryst. Growth* **243**, 503–516 (2002).

Acknowledgments

Funding: This research work is financially supported by a grant from the Ministry of Education of Singapore (R-284-000-197-114). H.H. is grateful to A*STAR for the financial support of his PhD program. **Author contributions:** H.H. carried out the experiments and analyzed the result. R.C. measured the stress-strain curves at different strain rates and different dimensions, the polarized UV-Vis spectra, and the stress-strain curves of PEDOT:PSS films with heat treating. S. Yue measured the Raman spectra. S. Yu and J.W. cosupervised the student and discussed the research work. J.O. conceived the idea and planned and supervised the research work. H.H. and J.O. wrote the manuscript. **Competing interests:** The authors declare that they have no competing interests. **Data and materials availability**: All data needed to evaluate the conclusions in the paper are present in the paper and/or the Supplementary Materials.

Submitted 2 May 2022
Accepted 6 October 2022
Published 25 November 2022
10.1126/sciadv.abq8160